Construction and Building Materials 411 (2024) 134714

Contents lists available at ScienceDirect

Construction and Building Materials

journal homepage: www.elsevier.com/locate/conbuildmat

Review

Bond behaviour of lap spliced GFRP bars in concrete members: A state-of-the-art review and design recommendations

Seyed Arman Hosseini [a], Ahmed Sabry Farghaly [a], Abolfazl Eslami [a], Antonio Nanni [b], Brahim Benmokrane [a,*]

[a] Department of Civil and Building Engineering, University of Sherbrooke, Quebec J1K 2R1, Canada
[b] Civil Engineering, University of Miami, Department of Civil and Architectural Engineering, 1251 Memorial Drive, Coral Gables, FL 33146, USA

ARTICLE INFO

Keywords:
Splice length
Splice Strength
Development length
Bond Strength
GFRP reinforcing bars

ABSTRACT

The expressions proposed in ACI 440.11–22, CSA S806–12, and CSA S6–19 to calculate the development length of glass fiber-reinforced polymer (GFRP) bars were mainly based on the procedure used for steel reinforcement. However, some assumptions were made due to the lack of extensive experimental data, and the effects of some parameters were disregarded. In this study, the accuracy of existing equations for the minimum splice length of GFRP bars embedded in concrete is evaluated using the results of 132 splice beam tests that experienced splitting failure with different characteristics, such as splice length, concrete cover, bar spacing, compressive strength of concrete, modulus of elasticity of bars, and confinement. This study employed multiple linear regression (MLR) analysis to develop a model with a selected dataset to predict the bond strength and minimum splice length of GFRP bars required to develop design stress. This offers a more accurate prediction of bond strength and the developed stress in spliced bars compared to current North American design codes. Using the proposed equation, minimum splice lengths were, on average, 6%, 22%, and 33% less than ACI 440.11–22 design code for effective concrete cover to bar diameter (c/d_b) ratios of 2.0, 2.5, and 3.0, respectively. In the presence of 8 mm diameter steel stirrups at spacing intervals of 50, 100, 200, and 300 mm, with c/d_b ratio of 2.0, the calculated minimum splice length using the proposed equation was, on average, 58%, 46%, 36%, and 32% less than ACI 440.11–22, respectively. Further research is needed to assess the impact of GFRP stirrup confinement within the splice region, varied staggering patterns, and recent advancements in the material and bond properties of GFRP bars on the bond strength of GFRP splices. These factors are currently not considered in existing design codes.

1. Introduction

The use of non-metallic reinforcement, such as glass fiber-reinforced polymer (GFRP) reinforcing bars, has become a widely accepted alternative to address the corrosion problem of steel reinforced concrete structures [1–3]. Aside from being corrosion resistant, GFRP bars have other desirable inherent advantages such as high strength-to-weight ratio, thermal insulation and lightness, electrical and magnetic neutrality, simplified on-site management, and lower lifetime maintenance costs compared to steel reinforcing bars [4–6]. In comparison to deformed steel bars, GFRP bars display a linear elastic response until failure, with a lower elastic modulus (25%−35% of elastic modulus of conventional steel) and provide different surface characteristics. Moreover, GFRP bars are more commonly utilized than aramid fiber-reinforced polymer (AFRP) and carbon fiber-reinforced polymer (CFRP), mainly due to their relatively lower costs [3,7,8].

The bond between GFRP bars and surrounding concrete is a crucial parameter that governs serviceability, cracking behavior, and ultimate capacity of GFRP reinforced concrete (RC) members [7,9]. Unlike deformed steel reinforcement, GFRP bars possess different mechanical and physical properties in their longitudinal and transverse directions and are produced with a variety of surface treatments which results in different force transfer mechanism between reinforcement and concrete [5,10,11].

Lap splicing—a commonly used and cost-effective method in construction for transferring force from one bar to another—is frequently required for GFRP bars due to their limited range of lengths influenced

* Correspondence to: Civil Engineering and Tier 1 Canada Research Chair Professor in Advanced Composite Materials for Civil Structures and Industrial Research Chair Professor in FRP Reinforcement for Sustainable & Resilient Concrete Infrastructure, Department of Civil & Building Engineering, University of Sherbrooke, Sherbrooke, Quebec, J1K 2R1, Canada.
E-mail address: Brahim.Benmokrane@usherbrooke.ca (B. Benmokrane).

https://doi.org/10.1016/j.conbuildmat.2023.134714
Received 31 August 2023; Received in revised form 18 December 2023; Accepted 20 December 2023
Available online 26 December 2023

Nomenclature

u	Average bond stress of GFRP bars to concrete (MPa)
$f_c^{'}$	Concrete compressive strength (MPa)
d_{cs}	Smaller of the distance from the bar center to closest concrete surface or two-thirds of center-to-center spacing of bars being developed (mm)
d_b	Nominal diameter of a bar (mm)
A_b	Cross-sectional area of a GFRP bar (mm^2)
A_{tr}	Cross-sectional area of transverse reinforcement (mm^2)
s	Spacing of transverse reinforcement (mm)
n	Number of bars being developed along the splitting plane
E_f	Modulus of elasticity of GFRP bars (GPa)
E_s	Modulus of elasticity of deformed steel bars (GPa)
k_1	Bar location factor
k_2	Concrete density factor
k_3	Bar size factor
k_4	Bar fiber factor
k_5	Factor to consider bar surface
l_d	Development length of GFRP bar in tension (mm)
l_s	Minimum splice length of GFRP bar in tension (mm)
f_d	Design stress in GFRP tension reinforcement at the ultimate limit state (MPa)
f_{cr}	Concrete cracking strength (MPa)
f_{fu}	Ultimate tensile strength of GFRP bars (MPa)
K_{tr}	Transverse reinforcement index representing contribution of confining reinforcement
f_y	Yield strength of transverse reinforcement (MPa)
c	Concrete cover to center of the bar or one-half of center-to-center spacing (mm)
α	Bar location factor for ACI 440.11–22

by manufacturing and transport considerations [12,13]. To provide reinforced concrete structural integrity, the section where bars are spliced needs to provide strength equal to or greater than that outside the spliced region. This is possible by providing an adequate splice length to sustain the design stress of reinforcement developed at the critical section (i.e. end of the spliced zone) [2]. Estimating the adequate splice length using an empirically based approach requires an extensive amount of data collected through experimental beam tests.

The splice strength of GFRP bars to concrete, defined as the maximum tensile strength at which rebar bond failure occurs, has been the subject of investigation in various studies. These studies have employed the splice beam test method and have taken into account a range of influential factors. These factors encompass splice length, bar diameter, concrete cover, bar spacing, confinement, surface treatment, bundling, as well as concrete type and compressive strength [2–7, 12–20]. Correspondingly, design codes for FRP reinforcement in the U. S., ACI 440.11–22 [6], and Canada, CSA S806–12 [21], and Chapter 16 of CSA S6–19 [22], include guidelines for bond mechanism in terms of embedment length. For tension lap splices, Canadian codes recommend a value of 1.3 times the development length in all cases, similar to the splice length suggested by ACI 318–19 [23] for steel bars. However, ACI 440.11–22 proposes differing values based on the spliced bar percentages and stress levels. This distinction is detailed in Table 25.2.2.1 of the aforementioned code.

The existing empirical equation proposed by ACI 440.11–22 [6] for development length calculation in FRP-reinforced concrete structures suffers from limitations due to the lack of available data on embedment or splice length. Consequently, conservative assumptions had to be made while disregarding the effects of some parameters. This approach resulted in an equation that may require excessive lap splice and development length for FRP bars, as reported in several recent studies [24–26]. Moreover, the current equation is based on test data that were conducted over two decades ago using FRP bars with surface deformations, such as a helical lug pattern or spiral wrap of fibers [27]. However, the bars used to develop this equation are no longer available today, and since its calibration, significant improvements have been made in FRP material properties and production methods.

Therefore, it is crucial to reassess the splice strength of lapped glass fiber reinforced polymer (GFRP) bars based on the outcomes of recent experimental studies available in the literature. This will provide a more representative equation for calculating the minimum splice length of new generation of GFRP bars embedded in concrete. The present study evaluates the accuracy of existing lap splice and development length equations for GFRP bars embedded in concrete by analyzing the results of 132 splice beam tests experienced splitting failure performed by previous researchers. This experimental data was then incorporated into a linear regression model by considering affecting parameters, to derive a more representative expression for estimating the optimum amount of splice length of GFRP bars. Finally, recommendations are made for future studies.

2. Database classification

Five general failure modes are expected in a given FRP-RC section with spliced bars, depending on various factors such as the splice length, reinforcement type, concrete properties, and reinforcement ratio. These modes include pullout of tensile reinforcements (slippage), concrete splitting, FRP rupture, concrete crushing, and concrete shear. If a specific splice length results in FRP rupture (in case of under-reinforced sections) or concrete crushing (in case of over-reinforced sections), it can be concluded that the minimum splice length is provided. However, the provided splice length may be much longer than or very close to the minimum splice length. If bond failure occurs, it is possible to extrapolate the minimum splice length that corresponds to a given stress in FRP bars from a limited number of test results. In practice, the pullout mode of failure, which may be due to a short splice length and/or high concrete cover to bar diameter ratio, is less likely to occur [28]. Therefore, the design of the test specimens is mainly based on selecting splice lengths that would fail in the bond splitting failure [2].

Previous studies have used various test methods to assess the experimental values for the average bond stress (u_{test}) acting on the surface of lapped GFRP bars. This is referred to as bond strength in this context. These methods include pullout tests, notched beam tests, hinged beam tests, beam end tests, and beam-splice tests. However, each method yields different bond strength results due to varying bond response characteristics. The pullout test is easy, quick, and cost-effective, but it cannot accurately represent the actual stress condition in flexural members. This is because it places the concrete around the reinforcing bar under compression while the bar itself is in tension, neglecting curvature effects present in real structural elements, thus leading to potential overestimation of bond strength.

On the other hand, the beam-splice test method offers a more realistic representation of the stress state in actual applications and considers curvature effects. Consequently, it provides a better evaluation of bond behavior in real-life scenarios. However, conducting this test on large-scale specimens can be expensive compared to other methods. Despite its cost, the beam-splice test method was efficient in previous research, making it a suitable choice for evaluating the bond behavior of lap-spliced GFRP bars in this study [2]. Hence, to evaluate the splice strength of GFRP reinforcing bars, a review of the technical literature related to the bond behavior of GFRP bars used splice beam test is presented in the following. Among previous studies, the results failed in

splitting are used to evaluate the accuracy of the current North American design codes (ACI 440.11–22, CSA S806–12, and CSA S6–19) and to propose a representative equation for estimating minimum splice length of GFRP bars.

Aly et al. [12] investigated the effects of bar diameter (15.9 and 19.1 mm) and splice length (ranged from 500 to 1100 mm) on the bond strength of sand-coated GFRP bars by testing 18 splice beams. Through analyzing the maximum theoretical stress in GFRP reinforcement, calculated based on maximal moment, they reported that the developed stress of spliced GFRP bars was linearly proportional to the splice length.

Mosley et al. [5] tested 6 lap splice beams to evaluate the effects of splice length (305 and 457 mm) and spliced bars clear spacing (25 and 120 mm) on the bond strength of GFRP bars having the bar diameter 15.9 mm. Fig. 1 provides the geometric and reinforcement details of the test specimens along with test set-up of spliced beams. Their findings outlined that the bond strength is proportional to the square root of the development length and is enhanced with increasing the elastic modulus of bars. Moreover, it was shown that increasing bar spacing changed the failure mode from side splitting to face splitting while the bond strength of GRFP bars is improved up to 50%.

Harajli and Abouniaj [16] carried out an experimental study consisting of 6 splice beam tests experienced concrete cover splitting mode with and without confinement using steel stirrups. All the specimens reinforced with 12 mm bar diameter with splice lengths of $15d_b$, $20d_b$, and $30d_b$ to investigate the bond behavior of GFRP bars in concrete. They concluded that GFRP bars resist 42–67% of their maximum tensile strength depends on their splice length. Moreover, it was shown that confinement has a significant effect in increasing the bond strength of GFRP bars by up to 31%.

The experimental program conducted by Choi et al. [17] on bond strength of GFRP bars in unconfined concrete indicated their lower bond strength compared to the conventional deformed steel bars. The test variables included splice length of $10d_b$ to $70d_b$, different cover thicknesses and bar spacing. Based on the results, the average bond strength decreases with increasing splice lengths, decreasing cover thicknesses or reducing bar spacing. A further study by Choi et al. [20] found that GFRP bars had an increased bond strength when the concrete cover and spacing between the bars were increased. This was confirmed by testing 11 GFRP reinforced beams with splice lengths of $45d_b$, $60d_b$, and $75d_b$.

Esfahani et al. [18] conducted another experimental study on the bond strength of GFRP bars by performing 11 splice beam tests. The experimental parameters were bar diameter (10, 12 and 16 mm), surface treatment (sand-coated and ribbed), splice length (varied from $18d_b$ to $33d_b$), concrete compressive strength (ranged from 41 to 72 MPa), and effect of confinement provide by stirrups within the splice region. It was found that the concrete compressive strength had no significant effect on the bond strength of the GFRP bars in spliced beams. In addition, they concluded that the bond strength of GFRP bars increases with decreasing bar diameter and using transverse reinforcement within the splice zone.

Pay et al. [19] carried out 28 splice tests on GFRP reinforced concrete beams with unconfined splice region to study the bond behavior of GFRP bars in concrete. The reinforcement details and test set-up used by them are shown in Fig. 2. It has been reported based on their study that bond strength of GFRP bars linearly increases with their axial rigidity (which is multiplied by elastic modulus and cross-sectional area). They also observed that the bond strength has a positive correlation with the elastic modulus of the reinforcing bars. Moreover, results of this study support a nonlinear relationship between bond strength and splice length as it can be noticed in Fig. 3. While previous research on relatively short splices [5] showed a square root relationship between bond strength and splice length for GFRP reinforcement, the longer splice lengths indicate that this relationship is significantly lower than the 0.5 power. They noted that this relationship is not constant and depends on the elastic modulus of the reinforcement.

Zemour et al. [3], tested six full-scale RC splice beams, each measuring 4300 mm in length, 250 mm in width, and 400 or 600 mm in height. The beams were reinforced with GFRP bars of 15.9 mm diameter (No.5) and subjected to four-point bending until failure. Two splice lengths of 20db and 40db (320 and 640 mm) were examined. Their results demonstrated a decrease in bond strength as the splice length increased, aligning with previous findings in the literature. Interestingly, they found that beam height could not significantly influence the bond strength of spliced reinforcing bars with relatively long splice lengths. Furthermore, they concluded that the design equations provided by JSCE-97 [29], CSA S806–12 [21], and ACI 440.1R-15 [30] can reasonably predict the splice length of GFRP bars in normal concrete. Among these, the provisions of JSCE-97 exhibited the highest safety

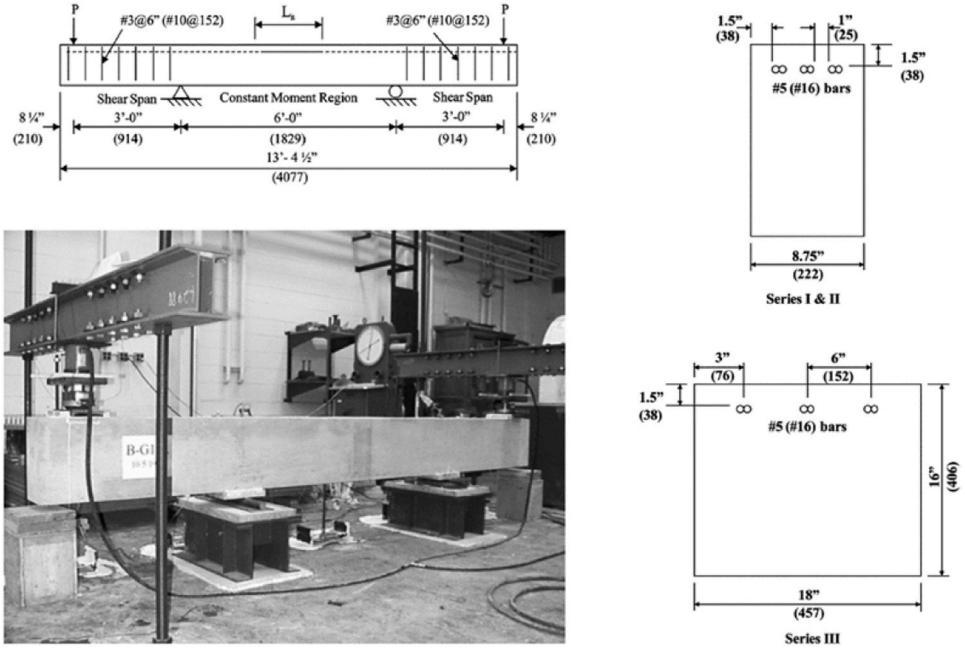

Fig. 1. The geometric dimensions, reinforcement details, and test set-up used by Mosley et al. [5].

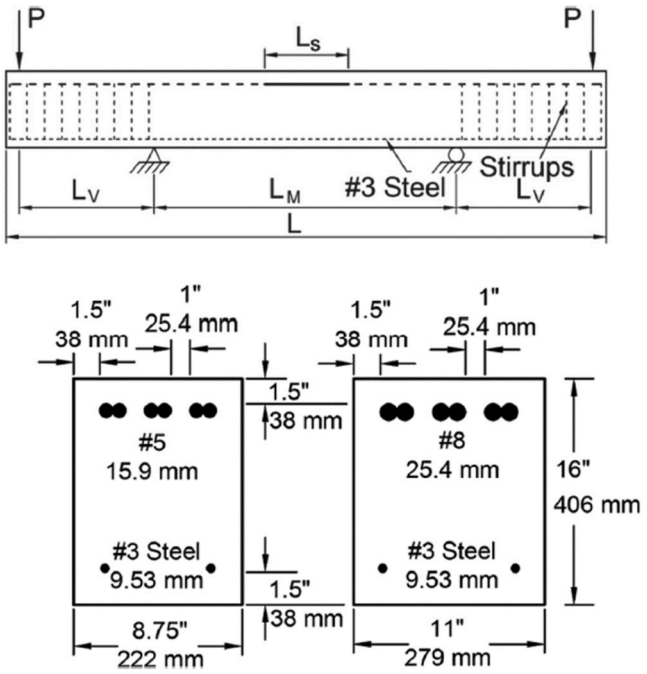

Fig. 2. The reinforcement details and test set-up used by Pay et al. [19].

margin. However, it was noted that the current CSA S6–14 provisions [31] led to a non-conservative prediction in most cases.

More recently, Wu et al. [7] examined 16 lap splice beams to investigate the bond performance of GFRP bars in concrete. Among the test parameters were the stirrup spacing, bar diameter, loading type, and the splice length of all specimens with bar diameters of 20 and 28 mm was 400 mm. Fig. 4 shows the reinforcement details of specimens. They reported that, due to confinement provided by stirrups, bond strength was significantly improved along the splice length compared to the specimens without stirrups and neglecting the contribution of confinement on bond strength of GFRP bars in design codes such as ACI 440.11–22 may lead to conservative value of development and splice length. Moreover, stirrups were found to contribute to the bond strength more effectively in the specimens reinforced with GFRP bars of 20 mm in diameter compared to those reinforced with GFRP bars of 28 mm in diameter. Thus, it is recommended that more stirrups be used in the FRP reinforced concrete structures with larger diameter of longitudinal reinforcement.

In another recent study, Al-Salloum et al. [13] conducted tests on six splice beams to investigate the achievable bar stress (f_f) given the existing embedment length, referred to as splice strength in this context. They used lap lengths of 40 times the rebar diameter in tension within constant moment regions. The test variables included two different stirrup spacing (50 and 100 mm) and two types of lapped splices: contact (with zero spacing) and non-contact (with 18 mm spacing) lapped splices. The results revealed that the lap length calculated based on ACI 440.1R-15 was overly conservative, particularly depending on the spacing of confining stirrups. Notably, the bond strength of GFRP rebars exhibited an increase with a decrease in the spacing of confining stirrups. Using confining stirrups led to a significant enhancement in bond strength, with improvements of 80% and 129% observed for 100-mm and 50-mm spacing of stirrups, respectively. Table 1 provides details of all tested specimens and their test results. The experimental splice strength ($f_{exp.}$) was calculated by multiplying the failure strain by the elastic modulus of the corresponding bars (E_f).

3. Current design codes

The following section presents a review of three North American design standards and guidelines on the normalized bond strength ($u/\sqrt{f'_c}$) between FRP bars and concrete, and minimum splice length for FRP bars.

3.1. CAN/CSA S806-12 (Canadian Standards Association 2012)

Canadian Standards Association, CSA S806–02 (2002), specifies the following equation for the average bond stress (u) of FRP bars to concrete in MPa:

$$u = \frac{d_{cs}\sqrt{f'_c}}{1.15(k_1k_2k_3k_4k_5)\pi d_b} \quad (1)$$

In Eq. (1), f'_c the concrete compressive strength in MPa; d_{cs} is the smaller of the distance from the center of the bar being developed to the closest concrete surface or two-thirds of the center-to-center spacing of bars being developed; d_b is the nominal diameter of a bar in mm; k_1 is bar location factor (1.3 for horizontal reinforcement placed more than 300 mm of fresh concrete is cast below the bar, 1.0 for all other cases); k_2 is concrete density factor (1.3 for structural low density concrete, 1.2 for structural semi-low-density concrete, 1.0 for normal-density concrete); k_3 is bar size factor (0.8 for $A_b < 300$ mm^2, 1.0 for $A_b < 300$ mm^2); k_4 is bar fiber factor (1.0 for CFRP and GFRP, 1.25 for AFRP); k_5 is a factor to consider bar surface (1.0 for surface roughened or sand coated or braided surfaces, 1.05 for spiral pattern surfaces or ribbed surfaces, 1.8 for indented surfaces). Based on the Eq. (1) for the average bond stress of FRP bars, CSA S806–12 [21] suggested the following equation for the minimum development length of FRP bars in tension in which the term $d_{cs} \le 2.5d_b$, and $\sqrt{f'_c} \le 5$ MPa.

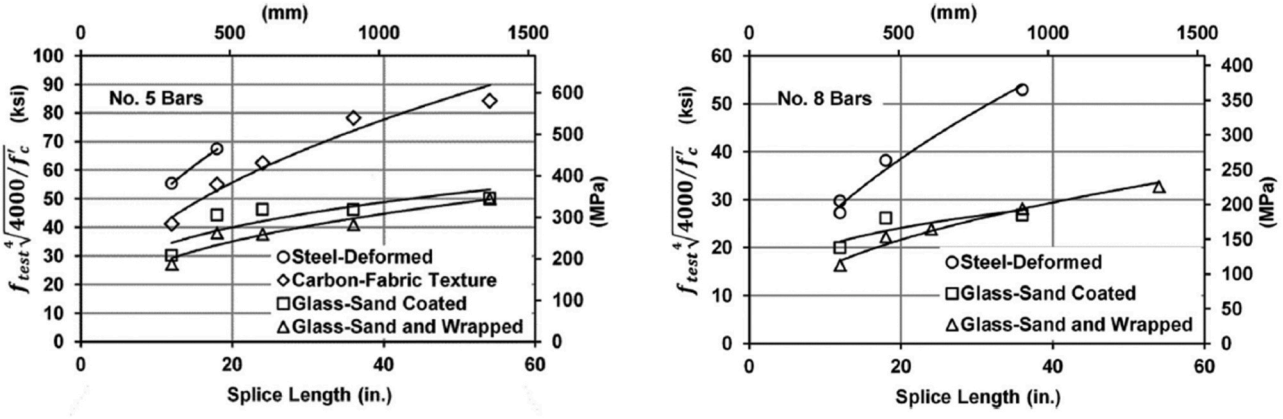

Fig. 3. Effect of splice length on normalized bond strength of No.5 and No.8 bars tested by Pay et al. [19].

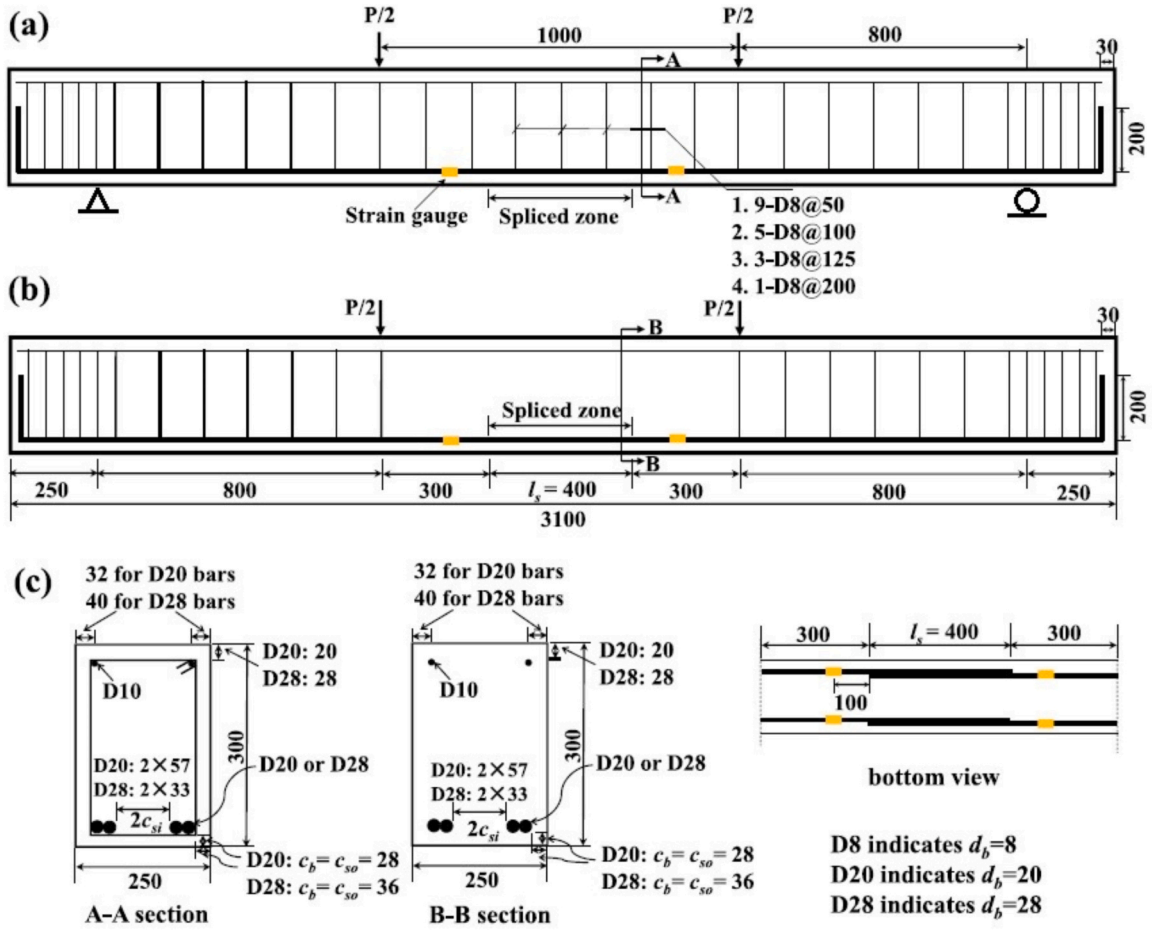

Fig. 4. The reinforcement details of splice beams tested by Wu et al. [7].

$$l_d = 1.15\frac{k_1k_2k_3k_4k_5}{d_{cs}} \times \frac{f_d}{\sqrt{f_c'}} \times A_b \tag{2}$$

In Eq. (2), l_d is development length of the FRP bar in tension; f_d is design stress in FRP tension reinforcement at the ultimate limit state in MPa; and A_b is the area of a bar. Based on CSA S806–12 [21], $1.3l_d$ is recommended to calculate the minimum splice length of FRP bars in tension.

3.2. CSA S6-19 (Canadian Highway Bridge Design Code 2019)

Canadian Highway Bridge Design Code, CSA S6–14 [31] recommends the following equation to estimate the average bond stress (u) of FRP bars to concrete in MPa in which the term $d_{cs} + K_{tr}\frac{E_{frp}}{E_s} \leq 2.5d_b$:

$$u = \frac{f_{cr}(d_{cs} + K_{tr}E_{frp}/E_s)}{0.45\pi d_b k_1 k_4} \text{where}: K_{tr} = \frac{A_{tr}f_y}{10.5sn} \tag{3}$$

Where f_{cr} is concrete cracking strength ($0.4\sqrt{f_c'}$) in MPa; d_{cs} is the smaller of the distance from the center of the bar being developed to the closest concrete surface or two-thirds of the center-to-center spacing of bars being developed; K_{tr} is transverse reinforcement index representing the contribution of confining reinforcement; E_{frp} and E_s denote the elastic modulus of FRP and steel bar in GPa, respectively; f_y is the yield strength of transverse reinforcement in MPa; s is maximum center-to-center spacing of transverse reinforcement within the embedment length; n is the number of bars being developed along the potential plane of splitting; d_b is FRP bar diameter; k_1 is bar location factor (1.3 for horizontal reinforcement placed more than 300 mm of fresh concrete is cast below the bar, 1.0 for all other cases); and k_4 is bar surface factor which is considered as the ratio of the bond strength of the FRP bar to that of a steel deformed bar with the same cross-sectional area as the FRP bar, but not greater than 1.0. In the absence of experimental data, k4 shall be taken as 0.8.

According to Eq. (3) for the average bond stress of FRP bars, CSA S6–19 [22] recommended the following equation for the required development length of FRP bars in tension based on the specified design tensile stress of FRP bar (f_d) in MPa where A_b is the cross-sectional area of a FRP bar:

$$l_d = 0.45\frac{k_1k_4}{d_{cs} + K_{tr}E_{frp}/E_s} \times \frac{f_d}{f_{cr}} \times A_b \text{where}: K_{tr} = \frac{A_{tr}f_y}{10.5sn} \tag{4}$$

Similar to CSA S806–12, CSA S6–19 [22] recommends 1.3 times of development length ($1.3l_d$) as minimum splice length of FRP bars in tension.

3.3. ACI 440.11-22 (ACI Committee 440 2022)

Based on ACI 440.11–22 [6], the normalized average bond stress acting on the surface of FRP bar ($u/\sqrt{f_c'}$) is determined through linear regression originally developed by Wambeke and Shield [27], based on 269 bond tests which yielded a valuable database covering beam-end tests, notch-beam tests, and splice tests. The normalized bond strength ($u/\sqrt{f_c'}$) is a function of the normalized concrete cover (c/d_b) and normalized embedment length (l_d/d_b), as described by the following equation:

Table 1
Test parameters and details of specimens.

	Specimen identification	f_c'	l_s	d_b	$\frac{l_s}{d_b}$	c	f_{fu}	E_f	Surface configuration	s	A_{tr}	$f_{exp.}$	$u_{exp.}$
		MPa	mm	mm		mm	MPa	GPa		mm	mm^2	MPa	MPa
Mosley et al.[5]	B-G1-1	38.6	457	15.9	28.7	20.5	607	40.5	W and S†	-	-	264	2.30
	B-G2-1	37.8	457	15.9	28.7	20.5	593	37.6	R*	-	-	224	1.95
	B-G1-2	29.0	305	15.9	19.2	20.5	607	40.5	W and S	-	-	199	2.59
	B-G2-2	27.0	305	15.9	19.2	20.5	593	37.6	R	-	-	203	2.65
	B-G1-3	41.2	305	15.9	19.2	46.0	607	40.5	W and S	-	-	340	4.43
	B-G2-3	40.9	305	15.9	19.2	46.0	593	37.6	R	-	-	322	4.20
Pay et al. [19]	B-PG-5-18	36.3	457	15.9	28.7	20.7	614	44.1	S**	-	-	326	2.84
	B-PG-5-36	37.7	914	15.9	57.5	20.7	614	44.1	S	-	-	344	1.50
	B-PG-5-24	32.0	610	15.9	38.4	20.7	614	44.1	S	-	-	331	2.16
	B-PG-5-24b	32.0	610	15.9	38.4	20.7	614	44.1	S	-	-	350	2.28
	B-PG-5-12	28.8	305	15.9	19.2	20.7	614	44.1	S	-	-	210	2.74
	B-PG-5-54	28.8	1372	15.9	86.3	20.7	614	44.1	S	-	-	349	1.01
	B-PG-5-12b	28.8	305	15.9	19.2	20.7	614	44.1	S	-	-	269	3.51
	B-HGO-5-18	36.3	457	15.9	28.7	20.7	490	40.0	W and S	-	-	227	1.97
	B-HGO-5-36	37.7	914	15.9	57.5	20.7	490	40.0	W and S	-	-	328	1.43
	B-HG1-5-18	36.3	457	15.9	28.7	20.7	676	44.1	W and S	-	-	281	2.44
	B-HG1-5-36	37.7	914	15.9	57.5	20.7	676	44.1	W and S	-	-	305	1.33
	B-HG1-5-24	32.0	610	15.9	38.4	20.7	676	44.1	W and S	-	-	269	1.75
	B-HG1-5-24b	32.0	610	15.9	38.4	20.7	676	44.1	W and S	-	-	291	1.90
	B-HG1-5-12	28.8	305	15.9	19.2	20.7	676	44.1	W and S	-	-	189	2.46
	B-HG1-5-54	28.8	1372	15.9	86.3	20.7	676	44.1	W and S	-	-	347	1.01
	B-HG1-5-12b	28.8	305	15.9	19.2	20.7	676	44.1	W and S	-	-	240	3.13
	B-HG2-5-24	32.0	610	15.9	38.4	20.7	793	50.3	W and S	-	-	328	2.14
	B-HG-8-18	36.3	457	25.4	18.0	25.4	524	39.3	W and S	-	-	163	2.26
	B-HG-8-36	37.7	914	25.4	36.0	25.4	524	39.3	W and S	-	-	210	1.46
	B-HG-8-12	27.7	305	25.4	12.0	25.4	524	39.3	W and S	-	-	112	2.33
	B-HG-8-12b	27.7	305	25.4	12.0	25.4	524	39.3	W and S	-	-	117	2.44
	B-HG-8-24	28.8	610	25.4	24.0	25.4	524	39.3	W and S	-	-	166	1.73
	B-HG-8-54	28.8	1372	25.4	54.0	25.4	524	39.3	W and S	-	-	228	1.06
	B-HG-8-24b	28.8	305	25.4	12.0	25.4	524	39.3	W and S	-	-	184	3.83
	B-PG-8-18	36.3	457	25.4	18.0	25.4	524	42.7	S	-	-	192	2.67
	B-PG-8-36	37.7	914	25.4	36.0	25.4	524	42.7	S	-	-	199	1.38
	B-PG-8-12	32.0	305	25.4	12.0	25.4	524	42.7	S	-	-	138	2.87
	B-PG-8-12b	32.0	305	25.4	12.0	25.4	524	42.7	S	-	-	127	2.64
	Specimen identification	f_c'	l_s	d_b	$\frac{l_s}{d_b}$	c	f_{fu}	E_f	Surface configuration	s	A_{tr}	$f_{exp.}$	$u_{exp.}$
		MPa	mm	mm		mm	MPa	GPa		mm	mm^2	MPa	MPa
Choi et al. [17]	B-2As-L10db-c25	30.0	127	13.6	9.3	32.2	690	40.8	HW†	-	-	178	4.76
	B-2As-L20db-c25	30.0	254	13.6	18.7	32.2	690	40.8	HW	-	-	281	3.76
	B-2As-L30db-c25	30.0	381	13.6	28.0	32.2	690	40.8	HW	-	-	322	2.87
	B-2As-L40db-c25	30.0	508	13.6	37.4	32.2	690	40.8	HW	-	-	357	2.39
	B-2As-L55db-c25	30.0	699	13.6	51.4	32.2	690	40.8	HW	-	-	501	2.44
	B-2As-L70db-c25	30.0	889	13.6	65.4	32.2	690	40.8	HW	-	-	513	1.96
	B-2Iso-L30db-c25	30.0	381	12.8	29.7	31.8	617	42.0	S	-	-	430	3.62
	B-2Iso-L40db-c25	30.0	508	12.8	39.6	31.8	617	42.0	S	-	-	467	2.95
	B-2Iso-L50db-c25	30.0	635	12.8	49.5	31.8	617	42.0	S	-	-	493	2.49
	B-2Iso-L60db-c25	30.0	762	12.8	59.5	31.8	617	42.0	S	-	-	521	2.19
	B-3K2-L15db-c25	23.0	191	12.0	15.9	31.4	692	37.2	S	-	-	292	4.60
	B-3K2-L30db-c25	23.0	381	12.0	31.8	31.4	692	37.2	S	-	-	393	3.09
	B-3K2-L45db-c25	23.0	572	12.0	47.6	31.4	692	37.2	S	-	-	509	2.67
	B-3K2-L60db-c25	23.0	762	12.0	63.5	31.4	692	37.2	S	-	-	542	2.13
	B-3K2-L30db-c13	23.0	381	12.0	31.8	18.7	692	37.2	S	-	-	381	3.00
	B-3K2-L30db-c51	23.0	381	12.0	31.8	36.0	692	37.2	S	-	-	431	3.39
	B-4K2-L30db-c25	23.0	381	12.0	31.8	29.1	692	37.2	S	-	-	364	2.86
	B-5K2-L30db-c25	23.0	381	12.0	31.8	20.2	692	37.2	S	-	-	385	3.03
	B-4K2-L45db-c25	23.0	572	12.0	47.6	29.1	692	37.2	S	-	-	399	2.09
	B-5K2-L45db-c25	23.0	572	12.0	47.6	20.2	692	37.2	S	-	-	437	2.29
	B-3As-L15db-c25	23.0	191	13.6	14.0	32.2	690	40.8	HW	-	-	248	4.42
	B-3As-L30db-c25	23.0	381	13.6	28.0	32.2	690	40.8	HW	-	-	305	2.72
	B-3As-L45db-c25	23.0	572	13.6	42.1	32.2	690	40.8	HW	-	-	336	2.00
	B-3As-L60db-c25	23.0	762	13.6	56.1	32.2	690	40.8	HW	-	-	415	1.85
Choi et al. [20]	3 F-L45-1.5	32.0	572	12.7	45.0	25.4	741	49.3	HW	-	-	378	2.10
	3 F-L45-2.0	32.0	572	12.7	45.0	31.4	741	49.3	HW	-	-	468	2.60
	3 F-L45-2.5	31.0	572	12.7	45.0	38.4	741	49.3	HW	-	-	499	2.77
	3 F-L60-2.0	30.0	762	12.7	60.0	31.4	741	49.3	HW	-	-	490	2.04
	3 F-L75-2.0	32.0	953	12.7	75.0	31.4	741	49.3	HW	-	-	591	1.97
	4 F-L45-1.5	30.0	572	12.7	45.0	25.4	741	49.3	HW	-	-	261	1.45
	4 F-L45-2.0	34.0	572	12.7	45.0	31.4	741	49.3	HW	-	-	308	1.71
	4 F-L45-2.5	34.0	572	12.7	45.0	31.4	741	49.3	HW	-	-	373	2.07
	5 F-L45-1.5	32.0	572	12.7	45.0	21.9	741	49.3	HW	-	-	232	1.29

(*continued on next page*)

Table 1 (*continued*)

	Specimen identification	f_c'	l_s	d_b	$\frac{l_s}{d_b}$	c	f_{fu}	E_f	Surface configuration	s	A_{tr}	$f_{exp.}$	$u_{exp.}$
		MPa	mm	mm		mm	MPa	GPa		mm	mm^2	MPa	MPa
	5 F-L45-2.0	30.0	572	12.7	45.0	21.9	741	49.3	HW	-	-	254	1.41
	5 F-L45-2.5	28.0	572	12.7	45.0	21.9	741	49.3	HW	-	-	286	1.59
Zemour et al.[3]	G-N-40-40d	39.0	636	15.9	40.0	38.0	762	50.0	S	-	-	420	2.63
	G-SC-40-40d	41.0	636	15.9	40.0	38.0	762	50.0	S	-	-	413	2.58
	G-N-60-40d	39.0	636	15.9	40.0	38.0	762	50.0	S	-	-	440	2.75
	G-SC-60-40d	41.0	636	15.9	40.0	38.0	762	50.0	S	-	-	392	2.45
	G-N-40-20d	39.0	318	15.9	20.0	38.0	762	50.0	S	-	-	287	3.59
	G-N-60-20d	35.5	318	15.9	20.0	38.0	762	50.0	S	-	-	348	4.35
	Specimen identification	f_c'	l_s	d_b	$\frac{l_s}{d_b}$	c	f_{fu}	E_f	Surface configuration	s	A_{tr}	$f_{exp.}$	$u_{exp.}$
		MPa	mm	mm		mm	MPa	GPa		mm	mm^2	MPa	MPa
Aly et al. [12]	5 G-50 N	49.0	500	15.9	31.4	48.0	590	40.0	S	-	-	508	4.04
	5 G-70 N	43.0	700	15.9	44.0	48.0	590	40.0	S	-	-	519	2.95
	6 G-50 N	41.0	500	19.1	26.2	49.6	560	37.0	S	-	-	377	3.60
	6 G-70 N	43.0	700	19.1	36.6	49.6	560	37.0	S	-	-	481	3.28
	6 G-80 N	41.0	800	19.1	41.9	49.6	560	37.0	S	-	-	553	3.30
	6G110N	41.0	1100	19.1	57.6	49.6	560	37.0	S	-	-	590	2.56
	6G70z	45.0	700	19.1	36.6	49.6	560	37.0	S	-	-	352	2.40
	6G70Z	43.0	700	19.1	36.6	49.6	560	37.0	S	-	-	372	2.54
	6G110Z	43.0	1100	19.1	57.6	49.6	560	37.0	S	-	-	394	1.71
	6G70L	43.0	700	19.1	36.6	49.6	560	37.0	S	300	100.5	432	2.95
	6G70N	43.0	700	19.1	36.6	49.6	560	37.0	S	150	100.5	481	3.28
	6G70M	45.0	700	19.1	36.6	49.6	560	37.0	S	50	100.5	556	3.79
	6G70N-KW	45.0	700	19.1	36.6	49.6	560	37.0	S	-	-	415	2.83
	6G70N-FX	43.0	700	19.1	36.6	34.6	560	37.0	S	-	-	466	3.18
	6G70N-KX	43.0	700	19.1	36.6	49.6	560	37.0	S	-	-	481	3.28
	6G70N-PX	45.0	700	19.1	36.6	51.4	560	37.0	S	-	-	427	2.91
	6G70N-KY	43.0	700	19.1	36.6	49.6	560	37.0	S	-	-	528	3.60
	6G70N-PY	45.0	700	19.1	36.6	51.4	560	37.0	S	-	-	471	3.21
Harajli and Abouniaj[16]	R1.25L15	48.0	180	12.0	15.0	21.0	500	37.0	R	-	-	210	3.51
	R1.25L20	48.0	240	12.0	20.0	21.0	500	37.0	R	-	-	256	3.21
	R2L15	48.0	180	12.0	15.0	31.0	500	37.0	R	-	-	215	3.58
	R2L20	48.0	240	12.0	20.0	31.0	500	37.0	R	-	-	292	3.65
	R1.25L30	52.0	360	12.0	30.0	21.0	500	37.0	R	-	-	271	2.25
	R1.25L20-C	52.0	240	12.0	20.0	21.0	500	37.0	R	80	100.5	336	4.20
Esfahani et al.[18]	S10-40-NC	41.0	180	10.0	18.0	30.0	700	37.0	S	-	-	485	6.73
	R16-40-NC	41.0	400	16.0	25.0	20.5	1000	60.0	R	-	-	218	2.18
	R16-40-S150	41.0	400	16.0	25.0	20.5	1000	60.0	R	150	100.5	320	3.20
	R16-40-S100	41.0	400	16.0	25.0	20.5	1000	60.0	R	100	100.5	418	4.18
	R16-40-S50	41.0	400	16.0	25.0	20.5	1000	60.0	R	50	100.5	518	5.18
	R12-40-S150	41.0	400	12.0	33.3	13.5	1000	60.0	R	150	100.5	575	4.31
	R12-40-S100	41.0	400	12.0	33.3	13.5	1000	60.0	R	100	100.5	685	5.14
	R12-40-S50	41.0	400	12.0	33.3	13.5	1000	60.0	R	50	100.5	829	6.22
	R12-70-S150	72.0	400	12.0	33.3	13.5	1000	60.0	R	150	100.5	559	4.19
	R12-70-S100	72.0	400	12.0	33.3	13.5	1000	60.0	R	100	100.5	685	5.14
	R12-70-S50	72.0	400	12.0	33.3	13.5	1000	60.0	R	50	100.5	885	6.64
Al-Salloum et al.[13]	B3	49.0	480	12.0	40.0	26.0	1286	52.0	R	-	-	492	3.08
	B4	49.0	480	12.0	40.0	26.0	1286	52.0	R	50	100.5	961	6.01
	B5	49.0	480	12.0	40.0	26.0	1286	52.0	R	100	100.5	869	5.43
	B6	49.0	480	12.0	40.0	26.0	1286	52.0	R	-	-	527	3.29
	B7	49.0	480	12.0	40.0	26.0	1286	52.0	R	50	100.5	990	6.19
	B8	49.0	480	12.0	40.0	26.0	1286	52.0	R	100	100.5	923	5.77
	Specimen identification	f_c'	l_s	d_b	$\frac{l_s}{d_b}$	c	f_{fu}	E_f	Surface configuration	s	A_{tr}	$f_{exp.}$	$u_{exp.}$
		MPa	mm	mm		mm	MPa	GPa		mm	mm^2	MPa	MPa
Wu et al.[7]	MG20-S50	55.9	400	20.0	20.0	38.0	696	51.1	R	50	100.5	335	4.18
	MG20-S100	55.9	400	20.0	20.0	38.0	696	51.1	R	100	100.5	337	4.21
	MG20-S125-1	55.9	400	20.0	20.0	38.0	696	51.1	R	125	100.5	282	3.53
	MG20-S125-2	55.9	400	20.0	20.0	38.0	696	51.1	R	125	100.5	262	3.28
	MG20-S125-3	55.9	400	20.0	20.0	38.0	696	51.1	R	125	100.5	270	3.37
	RG20-S125	55.9	400	20.0	20.0	38.0	696	51.1	R	125	100.5	280	3.49
	MG20-S200	55.9	400	20.0	20.0	38.0	696	51.1	R	200	100.5	221	2.77
	MG20-S0	55.9	400	20.0	20.0	38.0	696	51.1	R	-	-	192	2.40
	MG28-S50	55.9	400	28.0	14.3	47.0	650	48.8	HW	50	100.5	276	4.83
	MG28-S100	55.9	400	28.0	14.3	47.0	650	48.8	HW	100	100.5	299	5.24
	MG28-S125-1	55.9	400	28.0	14.3	47.0	650	48.8	HW	125	100.5	198	3.46
	MG28-S125-2	55.9	400	28.0	14.3	47.0	650	48.8	HW	125	100.5	195	3.41
	MG28-S125-3	55.9	400	28.0	14.3	47.0	650	48.8	HW	125	100.5	152	2.67
	MG28-S125-4	55.9	400	28.0	14.3	47.0	650	48.8	HW	125	100.5	196	3.44
	MG28-S200	55.9	400	28.0	14.3	47.0	650	48.8	HW	200	100.5	171	2.98
	MG28-S0	55.9	400	28.0	14.3	47.0	650	48.8	HW	-	-	165	2.89

†Wrapped and sand-coated
*Ribbed

* *Sand-coated
†Helically wrapped

$$\frac{u}{0.083\sqrt{f_c'}} = 4.0 + 0.3\frac{c}{d_b} + 100\frac{d_b}{l_d} \quad (5)$$

where f_c' is concrete compressive strength in MPa; c is the effective concrete cover which is the lesser of the cover to center of the bar being developed or one-half of the center-to-center spacing of bars being developed; d_b is the diameter of a FRP bar; and l_d is embedded length of FRP bar in concrete. The study predominantly used GFRP bars (240 out of 269 tests) with various bar surface conditions and diameters having the concrete compressive strength ranged from 28 to 45 MPa.

Using Eq. (5), ACI 440.11–22 [6] recommended the following equation for the required development length of FRP bar in tension in which the term $c/d_b \leq 3.5$:

$$l_d = \frac{\alpha\frac{f_d}{0.083\sqrt{f_c'}} - 340}{13.6 + \frac{c}{d_b}} \times d_b \quad (6)$$

In Eq. (6), l_d is FRP bar development length in tension; f_d is design stress in FRP bar; and α is bar location factor (1.5 for horizontal reinforcement placed more than 300 mm of fresh concrete is cast below the bar, 1.0 for all other cases). In contrast to two Canadian design codes, ACI 440.11–22 [6] has included a classification for the percentage of bars spliced at a section. This classification introduces Class A and B splices, which correspond to sections with 50% and 100% of bars spliced, respectively. ACI 440.11–22 [6] recommends using 1.0 and 1.3 times the development length as the necessary lap length for Class A and Class B splices in tension. It is worth noting that while this recommendation is similar to the approach used in ACI 318–19 [23] for the minimum splice length of steel bars, there is currently no experimental study available confirming this suggestion for GFRP bars. Therefore, further research may be necessary to investigate the effect of staggering distance and percentage of bars spliced at a section.

4. Evaluation of available design codes

Here a comparison has been conducted between the results of 132 splice beam tests which showed splitting failure in previous studies to assess the accuracy of current design codes in estimating of splice strength of GFRP bars. Table 1 presents the test parameters of 101 beams without stirrups and 31 beams confined using steel stirrups along the splice length. There is a range of lap splice lengths (l_s) from 127 mm to 1372 mm, bar diameters (d_b) from 12.0 mm to 25.4 mm, l_s/d_b from 10.0 to 86.3, concrete compressive strength (f_c') from 23 MPa and 72 MPa, ultimate nominal tensile strength (f_{fu}) of GFRP bars from 490 MPa to 1000 MPa, FRP bars elastic modulus (E_f) from 37 GPa to 60 GPa, stirrup spacing (s) from 50 mm to 300 mm, with stirrup's diameter of 8 mm for all tests. Fig. 5(a) to Fig. 5(f) compares the relationship between experimental splice strength of GFRP bars ($f_{exp.}$) with the theoretical predictions (f_p) of ACI 440.11–22, CSA S6–19, and CSA S806–12 design provisions by solving for f_d in Eq. 6, Eq. 4, and Eq. 2, respectively. It should be noted that the basic development length (l_d) for the calculation of GFRP bar stress was defined as $l_d = l_s/1.3$ considering the lap splice condition of the test specimens.

ACI 440.11–22 [6] predicts all test results with an average ratio of the test result to prediction ($f_{exp.}/f_{ACI440}$) equal to 1.05 and coefficient of variation (COV) of 0.307 which shows this design code slightly underestimates test results as it is shown in Fig. 5(b). The relatively large value of COV also indicates the predicted results are dispersed along with the whole range of l_s/d_b as it can be seen in Fig. 5(a). Furthermore, the results presented in Fig. 5(a) indicate that ACI 440.11–22 provides an acceptable estimation of the minimum splice length of GFRP bars for specimens without confinement. On the other hand, this design code obviously underestimates the results of almost all specimens having stirrups within the splice region, as the effect of confinement is not taken into account in this provision. As demonstrated in Fig. 5(d), the CSA S806–12 [21] considerably underestimates the developed stress in GFRP bars with an average ratio of the test result to prediction ($f_{exp.}/f_{CSA\ S806}$) of 1.26 and a coefficient of variation (COV) of 0.475. Moreover, as the ratio of splice length to bar diameter increased, the test result-to-prediction ratio decreased. This is due to non-uniform bond stress distribution, which leads to lower average bond strength by increasing the splice or development length [26].

This factor is disregarded by CSA S806, since the bond strength does not depend on embedment length as it can be noticed in Eq. (1). When the ratio splice length to bar diameter was greater than 40, CSA S806 overestimated all the test results. By separating test results of specimens with and without stirrups as it is illustrated in Fig. 5(c), it can be noticed that CSA S806–12 slightly overestimates the test results by increasing the developed stress in bars for specimens without confinement. On the other hand, for specimens having stirrups within the splice region, CSA S806–12 clearly underestimates the test results, as expected since this design code, like ACI 440.11–22, does not take the effect of confinement into account.

Fig. 5(f) indicates that CSA S6–19 [22] slightly overestimates the test results by showing an average ratio of the test result to prediction ($f_{exp.}/f_{CSA\ S6}$) equal to 0.96 and coefficient of variation (COV) of 0.407. Similar to CSA S806–12, as the ratio of splice length to bar diameter increased, the test result-to-prediction ratio decreased and when this ratio is higher than 40, CSA S6–19 overestimates almost all test results. By analyzing the test results separately as it can be seen in Fig. 5(e), it is evident that CSA S6–19 overestimated the test results by increasing the developed stress in bars in specimens without stirrups. Additionally, although the effect of stirrups within the splice region is considered in this design code by introducing transverse reinforcement index (K_{tr}), the test results were still slightly underestimated. This can be attributed to the fact that the confinement effect provided by the concrete cover and stirrups is limited to 2.5 times the bar diameter in this design code which needs to be corrected.

It can be concluded that all the current North American design codes need to be improved to be able to accurately estimate the ultimate stress developed by splicing GFRP bars, as the experimental to predicted values ($f_{exp.}/f_p$) are generally scattered. Nonetheless, ACI 440.11–22 provides more reliable predictions of splice strength compared to the other two design code for specimens without confinement. On the other hand, CSA S6–19 provides more accurate prediction of the experimental results for specimens having stirrups within splice region. The following section presents a proposed model for the average bond stress acting on the surface of GFRP bars. Consequently, a more representative equation is proposed for the minimum splice length of GFRP bars, covering the weaknesses of current design codes.

5. Proposed model to predict bond strength

The analysis of a dataset comprising 132 lap splice test results characterized by splitting failure looked at predicting the normalized bond strength ($u/\sqrt{f_c'}$) of spliced GFRP bars as the dependent variable. This prediction model was developed using a multiple linear regression (MLR) analysis. The analysis considered the effect of unitless parameters as independent variables that were shown, based on the available literature, to have an impact on the bond performance of GFRP bars. These parameters include the normalized splice length of GFRP bars (d_b/l_s), the normalized concrete cover and bar spacing (c/d_b), and the normalized confinement effect due to the presence of stirrups within the splice region (K_{tr}/d_b). The multiple linear regression (MLR) analysis

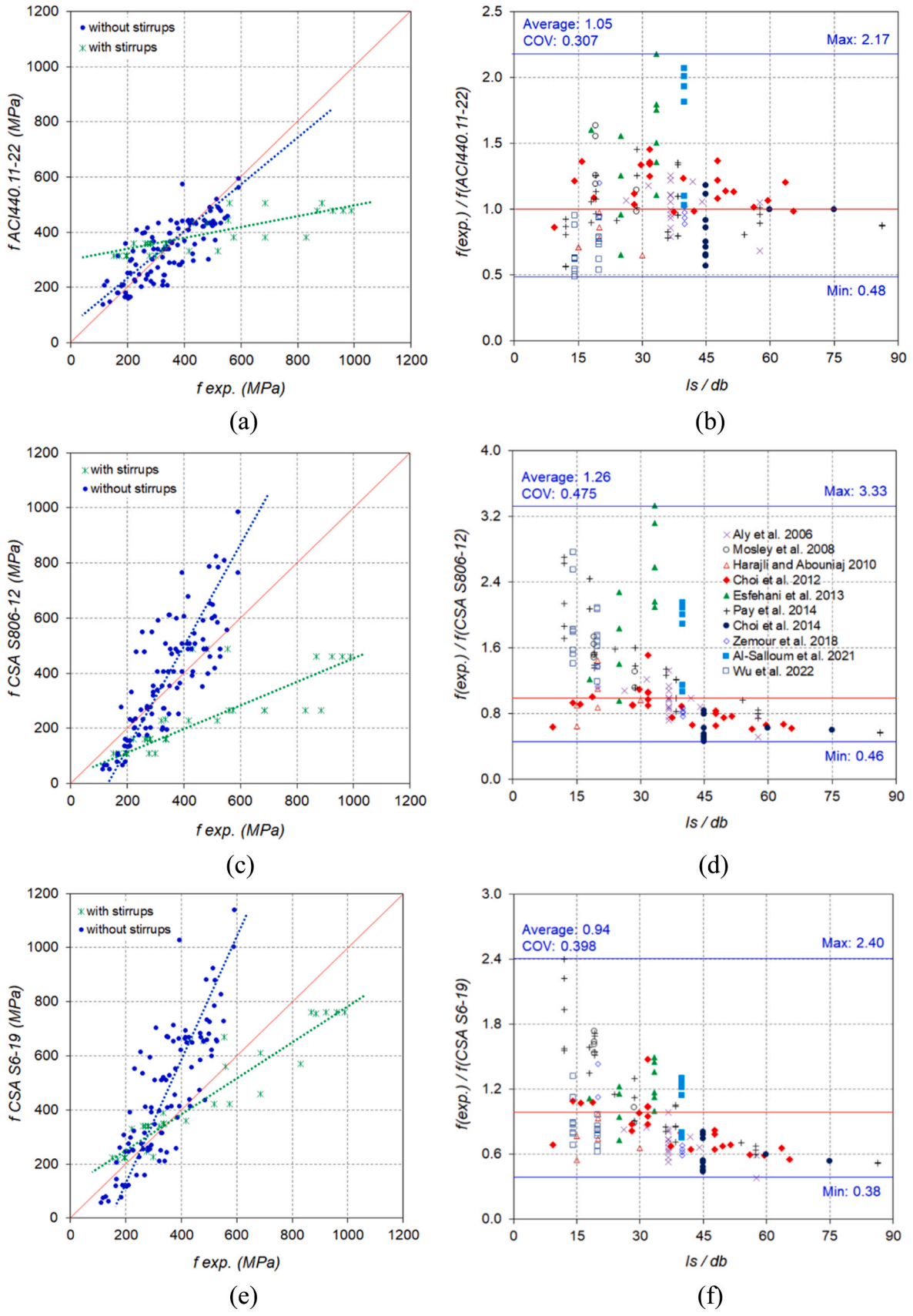

Fig. 5. Comparison of test results with prediction of (a-b) ACI 440.11–22 design method; (c-d) CSA S806–12 design method; (e-f) CSA S6–19 design method.

resulted in Eq. (7) as follows:

$$\frac{u}{\sqrt{f'_c}} = \frac{1}{k_1}\left(5.0\frac{d_b}{l_s} + 0.145\frac{c}{d_b} + 2.0\frac{K_{tr}}{d_b}\right) \text{where} : K_{tr} = 10\frac{A_{tr}}{sn}.\frac{E_f}{E_s} \quad (7)$$

It should be noted that c is the lesser of clear concrete cover (side and bottom) or one-half of the clear spacing of bars being developed; K_{tr} is a factor that represents the contribution of confining reinforcement across potential splitting planes which can be defined as the Eq. (7) where A_{tr} is the cross section area of GFRP bars; s is the spacing of transverse reinforcement; n is the number of bars being developed along the splitting plane; E_f is modulus of elasticity of GFRP bars; E_s is the modulus of elasticity of deformed steel bars, which is considered to be 200 GPa; and k_1 is a factor correspond for the effect of bar location which is set as 1.3 (for top bar casting position) and 1.0 (for bottom bar casting position). It is important to highlight that there is a scarcity of available data regarding the impact of GFRP stirrups on splice strength. Consequently, further experimental investigations are necessary to explore the effects of GFRP stirrups by readjusting the confinement index (K_{tr}).

Incorporating the candidate model requires verifying that the main assumptions underlying the linear regression model are satisfied. The first step involves checking the model prediction plot to determine if the relationship between observations and model predictions follows a linear pattern. Fig. 6(a) shows that this assumption is almost satisfied. Further investigation into the linearity of the model could be conducted by gathering more data placed at the higher tail of the plot, where higher bond strength values would be expected.

The next assumption pertains to the normality of the model, necessitating that the residuals adhere to a normal distribution. A quantile-quantile plot (Q-Q plot) serves as a tool to assess the conformity of model residuals to normality. If the points on the plot approximately form a straight diagonal line, the normality assumption is considered satisfied. Fig. 6(b) presents the Q-Q plot of the model, demonstrating that the proposed model satisfies the normality assumption, with residuals roughly following a normal distribution.

The other assumption of linear regression is that the residuals have constant variance at every level of predicted values, as well as the entire range of independent variable values, known as homoscedasticity. Figs. 7(a) to 7(c) show the values of residuals versus the values of the independent variables x_1, x_2, and x_3, which represent d_b/l_s, c/d_b, and K_{tr}/d_b, respectively. These plots show that the standardized residuals are scattered about zero with no clear pattern. Furthermore, Fig. 7(d) demonstrates that the prediction-to-observation ratios did not follow a specific pattern and are scattered uniformly about 1.0 within each level of predicted values. Based on these results, the proposed model satisfies all linear regression assumptions, including linearity, normality, and homoscedasticity.

By substituting the normalized bond strength $(u/\sqrt{f'_c})$ with the resulting stress in GFRP bars (f_d), the minimum splice length (l_s) to develop the corresponding stress can be calculated using Eq. (8) as follows. It is worth noting that Eqs. (7) and (8) are recommended for use when $c/d_b \leq 3$, as the database includes test data for c/d_b up to about 3. In cases where $c/d_b > 3$, additional experimental results are required to verify and update the equation. Moreover, since the dataset includes specimens with confinement having a maximum effective concrete cover to bar diameter c/d_b of 2.6, in situations where stirrups are present within the splice region, the value of c/d_b in Eqs. (7) and (8) should not exceed 2.5.

$$l_s = \frac{k_1\frac{f_d}{0.083\sqrt{f'_c}} - 240}{7.0\frac{c}{d_b} + 95.0\frac{K_{tr}}{d_b}} \times d_b \geq 250mm \text{where} : K_{tr} = 10\frac{A_{tr}}{sn}.\frac{E_f}{E_s} \quad (8)$$

As depicted in Fig. 6(a), the proposed equation for evaluating the bond strength of GFRP bars in concrete has led to a more accurate prediction compared to current design codes both in case of specimens with and without confinement stirrups. The estimated versus experimental values of developed stress in GFRP bars exhibit a linear relationship with correlation coefficient (R-factor) of 0.984. Moreover, proposed model predicts the test results with an average ratio of the test-to-prediction of developed stress in GRFP bars ($f_{exp.}/f_{prop.}$) of 1.00 ranging from 0.54 to 1.63 and coefficient of variation (COV) of 0.241. These findings are presented on Fig. 6(b), demonstrating a significantly more precise fit to the experimental data than current design provisions. Fig. 8.

Table 2 provides a statistical comparison of the experimental splice strengths with those predicted by the proposed analytical expression, as well as by selected design codes and previous models. The comparison is based on the average and coefficient of variation (COV) of the ratio of the test results to the splice strength predicted by the different methods.

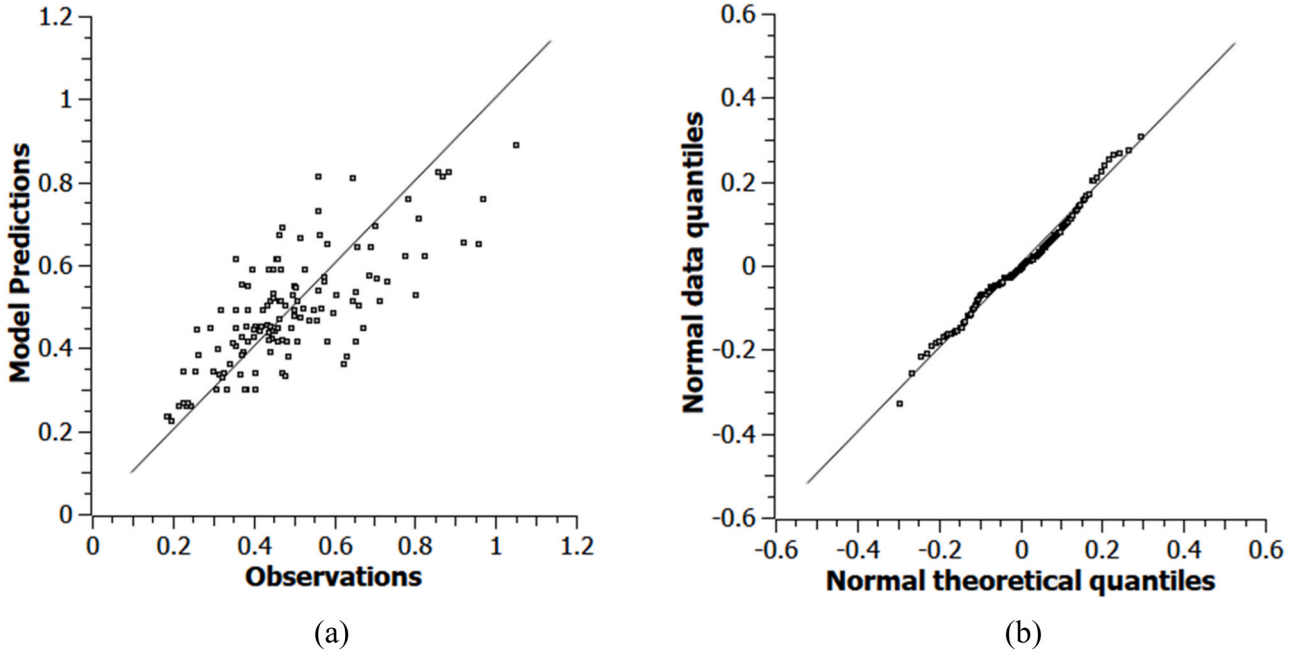

Fig. 6. Assessment of linear regression assumptions: (a) linearity check, (b) normality evaluation.

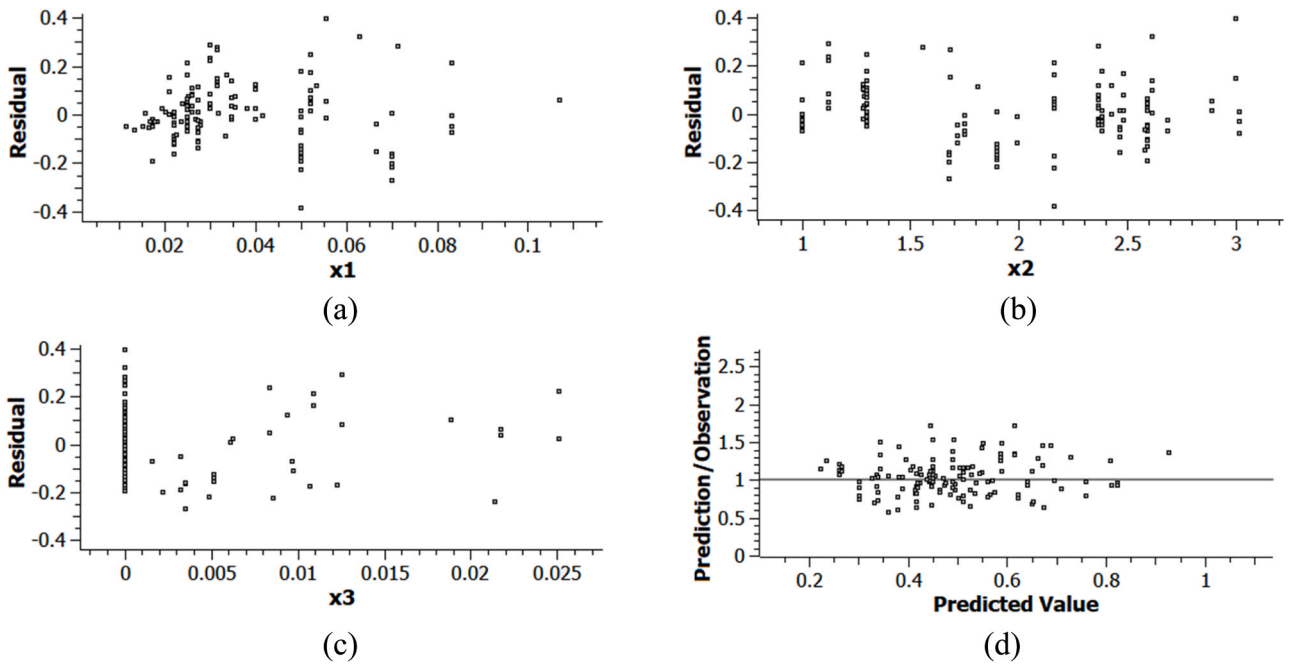

Fig. 7. Assessment of linear regression homoscedasticity assumption for: (a) $x_1 = d_b/l_s$; (b) $x_2 = c/d_b$; $x_3 = K_{tr}/d_b$; (d) predicted values.

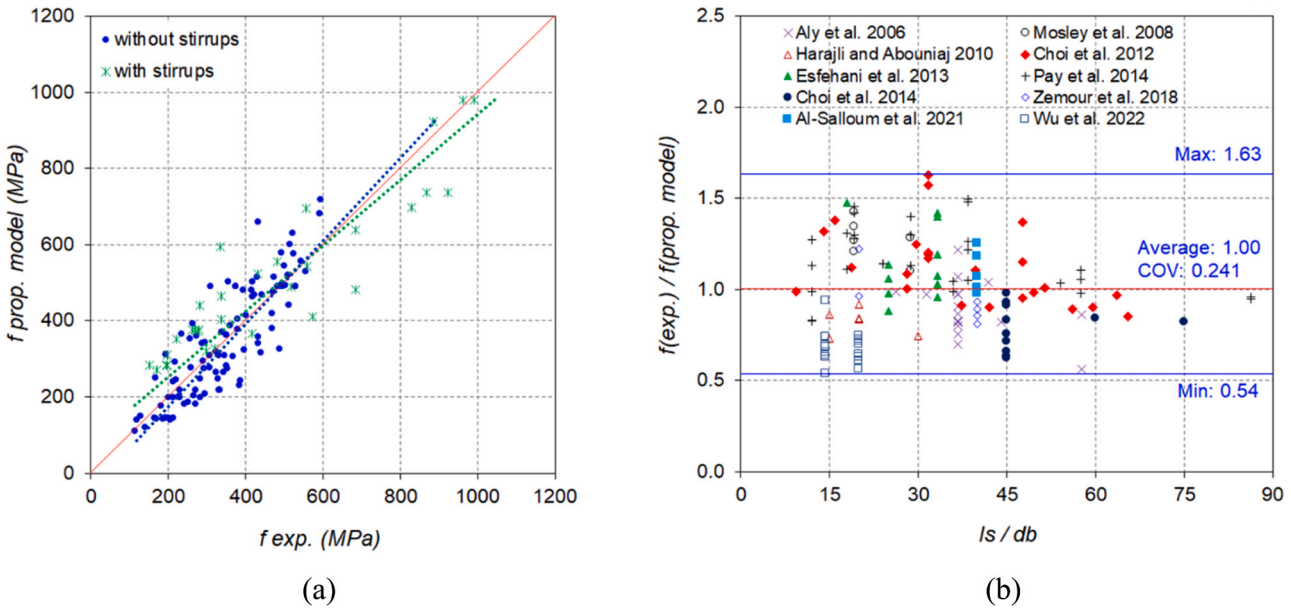

Fig. 8. Predicted to experimental values of stress in GFRP bar splices using linear regression model for specimens (a) with and without confinement; (b) tested in different studies.

Table 2
Comparison the theoretical and experimental splices strengths.

Method	Average Test-to-Prediction Ratio ($f_{exp.}/f_{prop.}$)	Coefficient of Variation (COV.)
Proposed model [Eq. (8)]	1.00	0.241
ACI 440.11-22[6]	1.05	0.307
CSA S806-12[21]	1.26	0.475
CSA S6-19[22]	0.94	0.398

The comparison of results reveal that using the proposed Eq. (8) to calculate the splice strength provides predictions with less scatter and greater accuracy than other methods. The average test-to-prediction ratio of splice strength calculated using Eq. (8) is 1.00. However, the average test-to-prediction ratio is 1.05, 1.26, and 0.94 for ACI 440.11–22, CSA S806–12, and CSA S6–19, respectively. Additionally, the proposed equation exhibits a lower coefficient of variation (COV) of 0.241 compared to the proposed equations by current design codes, which have COV values of 0.307 for ACI 440.11–22, 0.475 for CSA S806–12, and 0.398 for CSA S6–19. Accordingly, the proposed Eq. (8) demonstrates a more accurate prediction of the minimum splice length of GFRP bars required to develop a specific amount of design stress, compared to those provided by design codes.

As seen in Table 2, the proposed model and the model proposed by ACI 440.11–22 demonstrate greater accuracy in predicting the splice strength of GFRP bars compared to equations given by CSA S806–12 and CSA S6–19. Therefore, a comparison between the proposed Eq. (8), and Eq. (6) provided by ACI 440.11–22, considering 1.3 times the development length as the splice length, has been made in terms of the calculated minimum splice length of GFRP bars.

The results show that the proposed model predicted a minimum splice length shorter than that in ACI 440.11–22 for a range of design stress (f_d) from 500 to 1000 MPa, assuming a concrete strength of 40 MPa and an effective concrete cover to bar diameter (c/d_b) ranging from 2.0 to 3.0. To assess the effect of concrete-cover confinement, a comparison was made between the proposed model and ACI 440.11–22, as shown in Fig. 9(a). The proposed expression predicts the minimum splice length of GFRP bars to be approximately 6%, 22%, and 33% less than that of ACI 440.11–22 on average, for an effective concrete cover to bar diameter (c/d_b) of 2.0, 2.5, and 3.0, respectively.

In addition, the confinement effect of stirrups within the splice region was taken into consideration, assuming an effective concrete cover to bar diameter (c/d_b) ratio of 2.0 and a concrete strength of 40 MPa. The results showed that when steel stirrups with a diameter of 8 mm were used at spacing intervals of 50, 100, 200, and 300 mm, the proposed equation resulted in a minimum splice length of GFRP bars that was, on average, 58%, 46%, 36%, and 32% less than that stipulated by the ACI 440.11–22 design code, as shown in Fig. 9(b). Additionally, Fig. 10 demonstrates the simultaneous effect of concrete cover confinement (c/d_b), and stirrup spacing (s), on the ratio of minimum splice length calculated by the proposed Eq. (8) and Eq. (6) given by ACI 440.11–22 when assuming an average design stress (f_d) of 700 MPa. Fig. 10 illustrates that the proposed expression gives a lower splice length than ACI 440.11–22 when stirrups are used within the splice region for all ranges of effective concrete cover to bar diameter (c/d_b) values. The ratio of ($l_{s,prop.}/l_{s,ACI440}$) ranges from 0.42 to 0.68, 0.46 to 0.8, and 0.5 to 0.98 depending on the spacing of the stirrups for a given values of (c/d_b) equal to 2.5, 2.0, and 1.5, respectively. This can be attributed to the neglect of the influence of stirrup confinement along with the splice zone in ACI 440.11–22. It is worth noting that the dataset of specimens with stirrup confinement within the splice region has a maximum effective concrete cover to bar diameter (c/d_b) of 2.6. Beams with tight stirrup spacing and large cover might not be governed by splitting failure. Consequently, a comparison of given splice length was not made when (c/d_b) is greater than 2.5 and stirrups were used within the splice region.

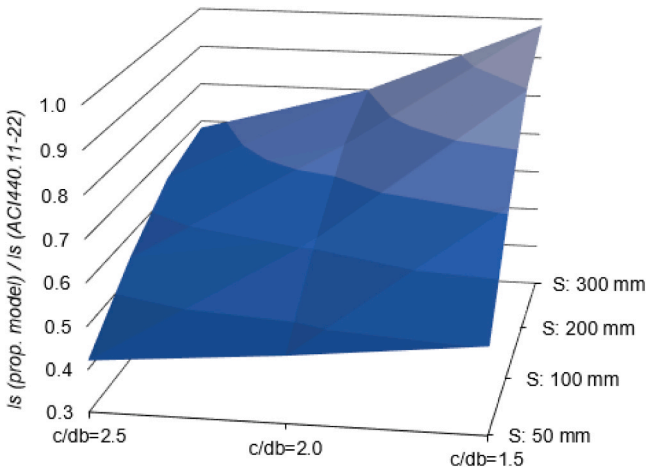

Fig. 10. The simultaneous effect of concrete cover confinement (c/d_b) and stirrup spacing (s) on the ratio of minimum splice length calculated by the proposed expression and ACI 440.11–22.

6. Conclusion

In this study, the accuracy of current design codes in evaluating the minimum splice length of GFRP bars in concrete was assessed by comparing the results of 132 splice beam tests that experienced splitting failure. Subsequently, multiple linear regression (MLR) analysis was conducted using the splice test results to develop a model predicting the bond strength and minimum splice length of GFRP bars in concrete. The prediction accuracy of this model was then compared to existing equations considering $l_d = l_s/1.3$ as it is suggested.

The parameters that were proven to affect the bond behavior of GFRP bars, such as concrete compressive strength (f'_c), embedment or splice length (l_s/d_b), the effect of concrete cover and spacing between adjacent bars (c/d_b), the influence of confinement due to the presence of stirrups within the splice region (K_{tr}/d_b), and the effect of bar location (k_1), were considered. Based on the obtained results, the following conclusions can be drawn:

- The study evaluates the performance of three North American design codes (ACI 440.11-22, CSA S806-12, CSA S6-19) in predicting the ultimate stress developed by lap spliced GFRP bars. ACI 440.11-22 design code slightly underestimates test results with a 1.05 average

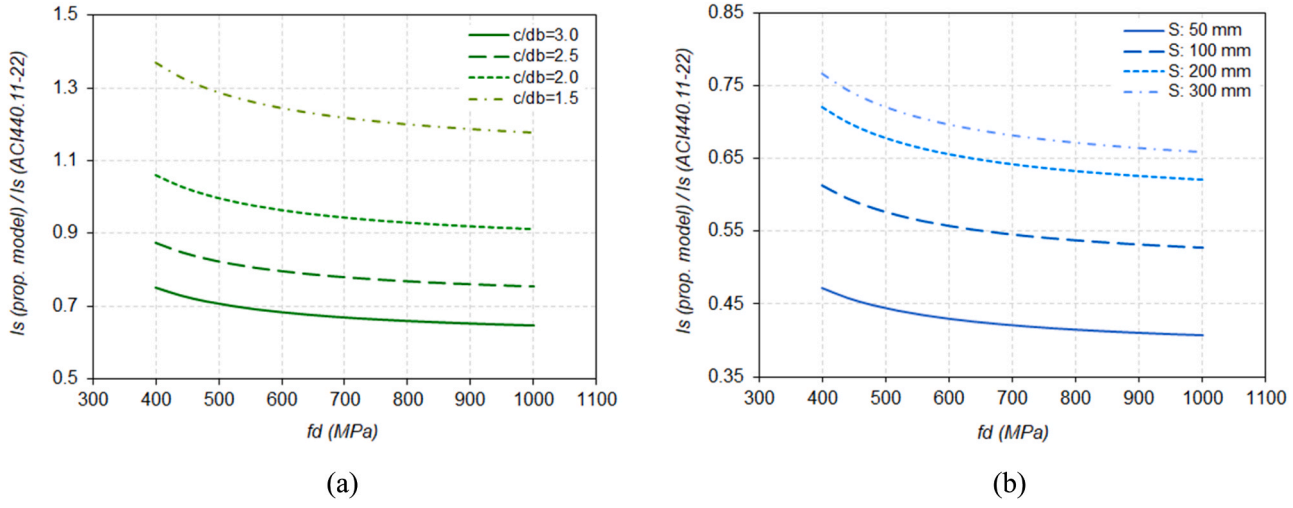

Fig. 9. Comparison of the minimum splice length (l_s) predicted by the proposed model and ACI 440 considering the effect of: (a) concrete cover (c/d_b); and (b) confinement spacing (s).

ratio of test result to prediction, and has a relatively high coefficient of variation (COV) of 0.307, indicating dispersed results. While it gives acceptable prediction for specimens without confinement, it underestimates results for specimens with stirrups.

- CSA S806-12 consistently underestimates GFRP bar stress, exhibiting an average test-to-prediction ratio of 1.26 and a coefficient of variation (COV) of 0.475. This underestimation is attributed to its neglect of non-uniform bond stress distribution, resulting in less accurate predictions as splice length increases. CSA S6-19 tends to overestimate test results, showing an average test-to-prediction ratio of 0.96 and a coefficient of variation (COV) of 0.407. Although this design provision considers the effect of stirrups, it still slightly underestimates results since CSA S6-19 imposes a limit on the maximum combined contribution of concrete cover and confinement (term $[d_{cs} + K_{tr}E_{frp}/E_s]$ in Eq. 4) to not be taken greater than $2.5d_b$.
- The proposed Eq. (7) have provided an evaluation bond strength of lap spliced GFRP bars in concrete and have led to a more accurate prediction of splice strength. The comparison between the current North American design codes and the proposed expression revealed that the proposed model provides more reliable and accurate prediction showing correlation factors (R-factor) of 0.984 between the predicted and experimental values of splice strength, while the average test-to-prediction ($f_{exp.}/f_{prop.}$) ratio and the coefficients of variation (COV) were 1.00, and 0.241 respectively.
- In contrast to ACI 440.11-22, the proposed model considers the influence of stirrup confinement within the splice region. The comparison of minimum splice lengths calculated by the proposed Eq. (8) and Eq. (6) provided by ACI 440.11-22 reveals an average reduction of 6%, 22%, and 33% for effective concrete cover to bar diameter (c/d_b) ratios of 2.0, 2.5, and 3.0, respectively. When stirrups are incorporated within the splice region at intervals of 50, 100, 200, and 300 mm, with (c/d_b) at 2.0, the model shows an average reduction of 58%, 46%, 36%, and 32% compared to ACI 440.11-22. The ratio of ($l_{s,prop.}/l_{s,ACI440}$) varies from 0.42 to 0.68, 0.46 to 0.8, and 0.5 to 0.98 for (c/d_b) values of 2.5, 2.0, and 1.5, respectively.

Declaration of Competing Interest

The authors confirm that there is no conflict of interest in this submission.

Data Availability

Data will be made available on request.

References

[1] T. Uomoto, H. Mutsuyoshi, F. Katsuki, S. Misra, Use of fiber reinforced polymer composites as reinforcing material for concrete, J. Mater. Civ. Eng. 14 (3) (2002) 191–209, https://doi.org/10.1061/(ASCE)0899-1561(2002)14:3(191).

[2] A. Asadian, A. Eslami, A.S. Farghaly, B. Benmokrane, Splice strength of staggered and non-staggered bundled glass fiber-reinforced polymer reinforcing bars in concrete, Acids Struct. J. 116 (4) (2019), https://doi.org/10.14359/51714482.

[3] N. Zemour, A. Asadian, E.A. Ahmed, K.H. Khayat, B. Benmokrane, Experimental study on the bond behavior of GFRP bars in normal and self-consolidating concrete, Constr. Build. Mater. 189 (2018) 869–881, https://doi.org/10.1016/j.conbuildmat.2018.09.045.

[4] M.R. Ehsani, H. Saadatmanesh, S. Tao, Design recommendations for bond of GFRP rebars to concrete, J. Struct. Eng. 122 (3) (1996) 247–254, https://doi.org/10.1061/(ASCE)0733-9445(1996)122:3(247).

[5] C.P. Mosley, A.K. Tureyen, R.J. Frosch, Bond strength of nonmetallic reinforcing bars, Acids Struct. J. 105 (5) (2008) 634–642, https://doi.org/10.14359/19947.

[6] ACI Committee 440. (2022). Guide for the design and construction of structural concrete reinforced with fiber-reinforced polymer (FRP) bars (ACI 440.11–22). American Concrete Institute, Farmington Hills, Michigan, USA.

[7] C. Wu, H.-J. Hwang, G. Ma, Effect of stirrups on the bond behavior of lap spliced GFRP bars in concrete beams, Eng. Struct. 266 (2022), 114552, https://doi.org/10.1016/j.engstruct.2022.114552.

[8] B. Basaran, I. Kalkan, A. Beycioglu, I. Kasprzyk, A Review on the Physical Parameters Affecting the Bond Behavior of FRP Bars Embedded in Concrete, Polymers 14 (2022) 1796, https://doi.org/10.3390/polym14091796.

[9] F. Yan, Z. Lin, M. Yang, Bond mechanism and bond strength of GFRP bars to concrete: a review, Compos B Eng. 98 (2016) 56–69, https://doi.org/10.1016/j.compositesb.2016.04.068.

[10] E. Cosenza, G. Manfredi, R. Realfonzo, Behavior and modeling of bond of FRP rebars to concrete, J. Compos. Constr. 1 (2) (1997) 40–51, https://doi.org/10.1061/(ASCE)1090-0268(1997)1:2(40).

[11] O. Gouda, A. Hassanein, K. Galal, Proposed development length equations for GFRP bars in flexural reinforced concrete members, J. Compos. Constr. 27 (1) (2023), https://doi.org/10.1061/(ASCE)CC.1943-5614.0001272.

[12] R. Aly, B. Benmokrane, U. Ebead, Tensile lap splicing of fiber-reinforced polymer reinforcing bars in concrete, Acids Struct. J. 103 (6) (2006) 857–864, https://doi.org/10.14359/18239.

[13] Y. Al-Salloum, L. Alaoud, H. Elsanadedy, A. Albidah, T. Almusallam, H. Abbas, Bond performance of GFRP Bar-splicing in reinforced concrete beams, J. Compos. Constr. 26 (2) (2022), https://doi.org/10.1061/(ASCE)CC.1943-5614.0001190.

[14] B. Tighiouart, B. Benmokrane, P. Mukhopadhyaya, Bond strength of glass FRP rebar splices in beams under static loading, Constr. Build. Mater. 13 (7) (1999) 383–392, https://doi.org/10.1016/S0950-0618(99)00037-9.

[15] Aly, R. (2005). Experimental and analytical studies on bond behaviour of tensile lap spliced FRP reinforcing bars in concrete. PhD, University of Sherbrooke, Sherbrooke, QC, CA.

[16] M. Harajli, M. Abouniaj, Bond performance of GFRP bars in tension: experimental evaluation and assessment of ACI 440 guidelines, J. Compos. Constr. 14 (6) (2010) 659–668, https://doi.org/10.1061/(ASCE)CC.1943-5614.0000139.

[17] D.-U. Choi, S.-C. Chun, S.-S. Ha, Bond strength of glass fibre-reinforced polymer bars in unconfined concrete, Eng. Struct. 34 (2012) 303–313, https://doi.org/10.1016/j.engstruct.2011.08.033.

[18] M.R. Esfahani, M. Rakhshanimehr, S.R. Mousavi, Bond strength of lap-spliced GFRP bars in concrete beams, J. Compos. Constr. 17 (3) (2013) 314–323, https://doi.org/10.1061/(ASCE)CC.1943-5614.0000359.

[19] A.C. Pay, E. Canbay, R.J. Frosch, Bond strength of spliced fiber-reinforced polymer reinforcement, Acids Struct. J. 111 (2) (2014), https://doi.org/10.14359/51686519.

[20] Y.C. Choi, K.H. Cho, B.I. Bae, H.K. Choi, Experimental study on the performance of tensile lap-spliced GFRP rebars in concrete beam, Mag. Concr. Res. 66 (24) (2014) 1250–1262.

[21] Canadian Standards Association (2012). Design and construction of building structures with fiber reinforced polymers (CAN/CSA S806–12). Canadian Standards Association, Ontario, Canada.

[22] Canadian Standards Association (2019). Canadian Highway Bridge Design Code (CAN/CSA S6–19). Canadian Standards Association, Ontario, Canada.

[23] ACI 318–19: Building Code Requirements for Structural Concrete and Commentary. American Concrete Institute, Michigan, USA, 2019.

[24] S. Islam, H.M. Afefy, K. Sennah, H. Azimi, Bond characteristics of straight- and headed-end, ribbed-surface, GFRP bars embedded in high-strength concrete, Constr. Build. Mater. 83 (2015) 283–298, https://doi.org/10.1016/j.conbuildmat.2015.03.025.

[25] V. Benzecry, A. Ruiz Emparanza, F. De Caso y Basalo, A. Nanni, Bond coefficient, kb, of GFRP bars, Constr. Build. Mater. 292 (123380) (2021), https://doi.org/10.1016/j.conbuildmat.2021.123380.

[26] E. Makhmalbaf, A.G. Razaqpur, Development length of glass fibre reinforced polymer (GFRP) rebar based on non-uniform Bond Stress, Can. J. Civ. Eng. 49 (3) (2022) 420–431, https://doi.org/10.1139/cjce-2020-0400.

[27] B.W. Wambeke, C.K. Shield, Development length of glass fiber-reinforced polymer bars in concrete, Acids Struct. J. 103 (1) (2006) 11–17, https://doi.org/10.14359/15081.

[28] Joint ACI-ASCE Committee 408, Bond and Development of Straight Reinforcing Bars in Tension (ACI 408R-03), American Concrete Institute, Farmington Hills, MI, 2003, 49 pp.

[29] Japan Society of Civil Engineers. Recommendation for design and construction of concrete structures using continuous fiber reinforcing materials (JSCE-1997). Tokyo, Japan; 1997.

[30] ACI Committee 440, Guide for the Design and Construction of Structural Concrete Reinforced with Fiber-Reinforced Polymer (FRP) Bars (ACI440.1R-15), American Concrete Institute, Farmington Hills, MI, 2015.

[31] Canadian Standards Association. Canadian Highway Bridge Design Code (CSA-S6–14). Mississauga, Ontario, Canada; 2014.